Nonequilibrium Fluctuations in Metaphase Spindles: Polarized Light Microscopy, Image Registration, and Correlation Functions

Jan Brugués and Daniel J. Needleman

School of Engineering and Applied Sciences, Department of Molecular and Cellular Biology, FAS Center for Systems Biology, Harvard University, 52 Oxford Street Cambridge, MA 02138 USA

ABSTRACT

Metaphase spindles are highly dynamic, nonequilibrium, steady-state structures. We study the internal fluctuations of spindles by computing spatio-temporal correlation functions of movies obtained from quantitative polarized light microscopy. These correlation functions are only physically meaningful if corrections are made for the net motion of the spindle. We describe our image registration algorithm in detail and we explore its robustness. Finally, we discuss the expression used for the estimation of the correlation function in terms of the nematic order of the microtubules which make up the spindle. Ultimately, studying the form of these correlation functions will provide a quantitative test of the validity of coarse-grained models of spindle structure inspired from liquid crystal physics.

Keywords: Spindle, Microtubule, Image Registration, Correlation Function, Active Liquid Crystal

1. INTRODUCTION

The spindle is a highly dynamic assembly responsible for the proper segregation of the genetic material to the daughter cells during cell division.[1] Like many other sub-cellular structures, the spindle exists in a non-equilibrium steady state, and requires a constant flux of energy and matter to maintain its shape.[2] Understanding the spindle is not only crucial for cell biology, but it also poses a fundamental challenge for physics since spindles behave drastically differently from non-living materials that have traditionally been studied.

The body of the spindle is composed of rigid polymers, called microtubules, a number of proteins which influence microtubule assembly and disassembly, motors and other proteins which cross-link and organize the microtubules, and a variety of regulatory proteins.[3] While many of the molecules that make up the spindle are known, it is still unclear how these components work together to determine the morphology and behaviors of the spindle. While ultimately it would be desirable to have a complete, microscopic theory of the spindle and all its constituents, such a goal seems very distant at present. An alternative approach to understanding the spindle is to attempt to formulate a phenomenological model, capable of capturing general features such as spindle shape, size, or response to external perturbations by considering force balance, mass conservation, and equations for relevant coarse grained fields. Similar approaches have been highly successful in studying non-living soft materials, such as liquid crystals and membranes.[4]

Amongst all the components that form the spindle, microtubules are ultimately responsible for its mechanical and structural properties. Therefore, microtubule density and orientation are good candidate fields for a phenomenological theory describing the spindle. Previous theoretical studies have constructed hydrodynamic descriptions of mixtures of motors and microtubules.[5,6] Other works use a rather less coarse grained models in which microtubules are considered as rigid rods moved by motors.[7,8] However it is unclear if such simple descriptions are relevant for understanding complex biological structures such as the spindle. In order to test if these models are valid for the spindle, and more fundamentally, if there is even the possibility for a coarse grained

Further author information: (Send correspondence to JB)
JB: E-mail: jbrugues@fas.harvard.edu
DJN : E-mail: dan_needleman@harvard.edu

description for the spindle in general, it is necessary to perform a detailed comparison between quantitative experiments and theory.

Polarized light microscopy is a powerful tool for non-invasive observations of microtubule structure and dynamics in spindles.[9] Shinya Inoue, who performed the first thorough studies of spindles with polarized light, was so struck by the characteristic flickering of spindle birefringence that he gave the phenomena its own name, calling it "the northern lights" after the fluctuations of the aurora borealis.[10] These dynamics are still not understood. We believe that an analysis of fluctuations in spindle birefringence will provide a means to test the validity of coarse-grained theories, in analogy with previous studies of the flickering of red blood cells,[11] where measurements of correlation functions have led to deep insights into membrane physics.

In this paper, we present a method to measure fluctuations of microtubule orientations in spindles using quantitative polarized light microscopy (LC-Polscope[12]). We provide a detailed description of registration algorithms to correct for motions of the spindle during acquisition, the proper definition of the orientational order parameter, and appropriate methods to compute the correlation functions.

2. MATERIALS AND METHODS

2.1 Spindle assembly from *Xenopus Laevis* Egg extracts and sample preparation

CSF-arrested egg extracts were prepared from *Xenopus Laevis* female oocytes. Cycled spindles were assembled as described in.[13,14] Briefly: demembrenated sperm and calcium where added to extracts, resulting in the formation of nuclei. The reactions where then driven into metaphase by addition of metaphase-arrested extract, and spindles formed after 1.5 hr at 18°C .

For imaging, a small aliquot of extract ($\sim$5 μl) was spread with a micropipette tip over an open chamber made of a cutout metal slide and a 22 mm coverslip, and covered with mineral oil to prevent evaporation. The chamber was mounted on an inverted microscopy equipped with an LC-Polscope.

2.2 Imaging

Imaging was performed with an LC-Polscope,[12] which makes use of a liquid crystal based universal compensator to generate light of defined ellipticity, a circular analyzer, and quantitative algorithms .[12] For each pixel in an image, the LC-Polscope measures the retardance - the sample birefringence integrated over the optical volume - and the orientation of the optical slow axis. Sato et al.[9] showed that the birefringence observed in the spindle is caused by its microtubules. The measured retardance is determined by the number of microtubules in an optical volume and their degree of alignment. The optical axis is the direction in which the microtubules are aligned. For coarse-grained theories, the dynamics of the optical axis is particularly interesting because, in analogy with liquid crystal theories, it is expected to be a slow variable relevant to the systems large scale dynamics.[4] We therefore focus on measuring correlations functions of the slow axis in spindles.

An image obtained with the LC-Polscope is shown in Fig. 1. In order to observe the temporal evolution of a spindle, we acquired movies, typically five minutes long, by taking images every two seconds. During the course of a movie the spindle moves around considerably, most likely due to convective flows in the chamber and the action of motors incorporated on the surface of the coverslip, Fig. 2(A). When computing correlations, we need to compare the same point in the spindle at different times, therefore a proper registration of the different frames with respect to each other is crucial for the correct interpretation for the correlation functions. For the rest of the paper, we will discuss an algorithm for the accurate registration of the spindle, and we will develop an appropriate means of measuring the spatio-temporal correlation function of orientation fluctuations in the spindles.

3. ALIGNMENT PROCEDURE

The registration of two images that are translated, rotated or scaled with respect to one another is a fundamental problem in image acquisition and processing. There are several registration strategies in the literature which include methods based on correlations, Fast Fourier Transform-based methods,[15] and feature-based methods.[16] The images we need to register are frames acquired at different times. Since consecutive frames are inevitably

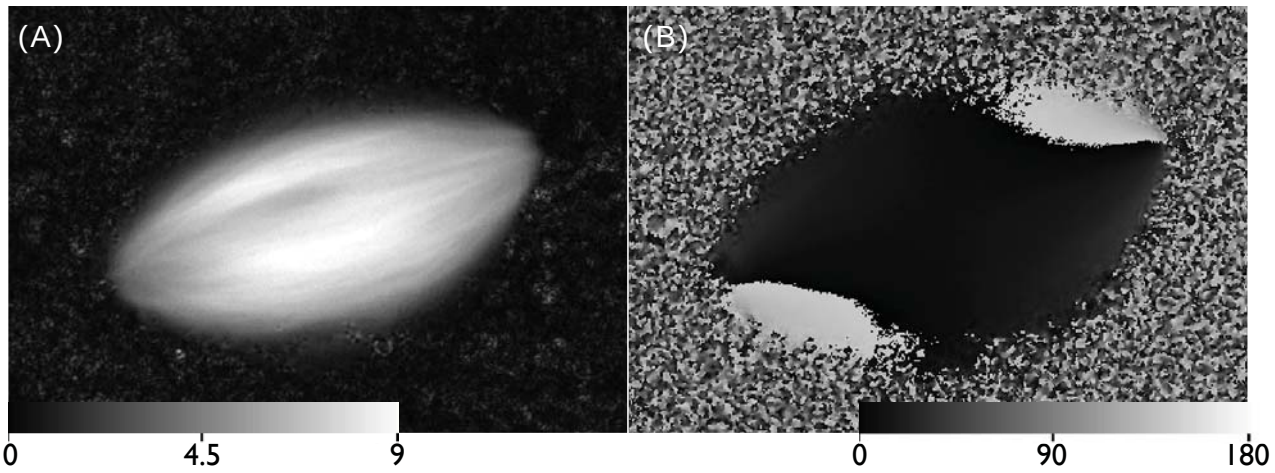

Figure 1. Spindle images obtained using the LC-Polscope.[12] (A) retardance image, scale bar in nanometers. (B) orientation image, scale bar in degrees.

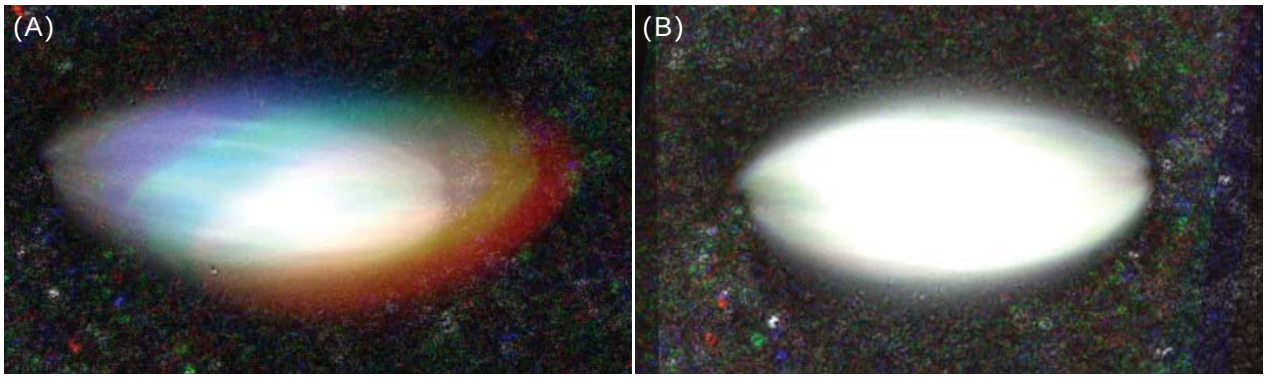

Figure 2. Result of the alignment algorithm. (A) Superposition of four frames of the raw data (at times 0, 48 seconds, 98 seconds, 149 seconds) in red, green, blue and grey associated colors. (B) Superposition of the same frames with the same colors as in (A) after being aligned using the algorithm described in the text.

different, there cannot be a fully objective, absolute measure of alignment quality. The challenge is to find a good registration algorithm and methods to estimate its accuracy.

There are two immediate candidates to use as alignment methods. One is a spindle shape based method. Using the boundary of the spindle as a reference, we can find the orientation and translation of a frame with respect to another reference frame (typically by means of an ellipsoidal fit and the computation of the center of mass). Although intuitive and simple, this method performs poorly because the internal dynamics of the spindle causes slight shape changes overtime, see Fig. 5. The resulting poorly aligned stacks inevitably show a characteristic flickering, which corresponds to errors in the alignment of several pixels and degrees.

An alternative to this method is the use of a frame to frame bulk correlation method, with the hope that even though fluctuations are significant, the internal features of the spindle are robust enough to provide an accurate alignment. In most applications, registration approaches involve correlation of the full images. In our case, we need to segment the image to prevent misalignment of the spindle by motions of vesicles and other background features. This is achieved by a shape recognition algorithm, consisting of an image thresholding (see paragraph below), which is used as a mask to compute the correlation only in the interior of the spindle. As noted previously, the overall shape of the spindle changes overtime due to strong fluctuations in the boundary. Moreover, we do not want any errors in determining the shape to propagate in the registration. As a consequence we need to make sure that the correlations in our algorithm are computed in a fashion that is insensitive to the changing of shape of the spindle, the particular method of obtaining its shape, and the shape overlap between consecutive frames.

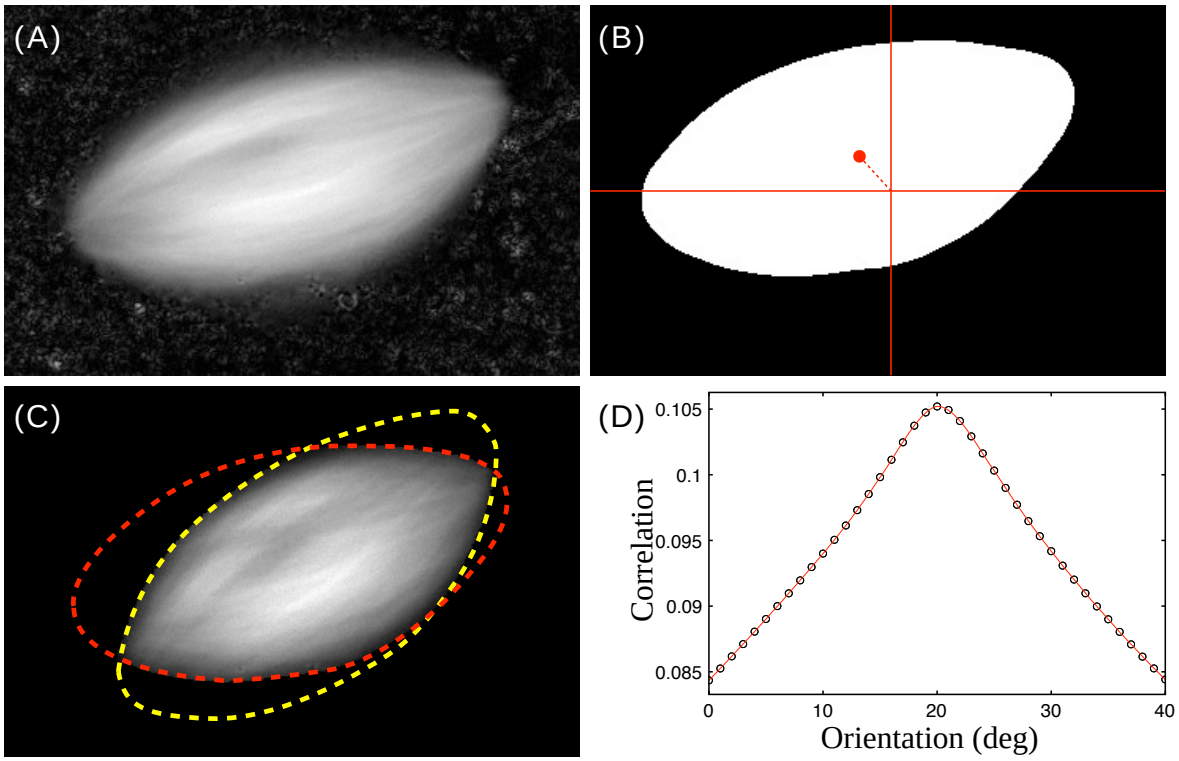

Figure 3. Key steps in the registration algorithm. For each frame (A), we find its corresponding mask and center of mass (B). The mask is used to filter the background. The image is then rotated by a set of discrete angles (-10 to 10 in steps of 0.5 deg), and correlated with the previous frame for every image translation (C). The maximum value of the correlation for each angle is fitted to a spline and the angle that registers the two frames is obtained by finding maximum of the fitted correlation (D).

3.1 Description of the algorithm

The result of the algorithm is a new stack of aligned frames. Starting from the second frame, each frame is compared to its predecessor, and a displacement and rotation magnitude are stored. The images are only aligned after the entire algorithm has completed. Updating the alignment for each frame directly after determining its rotation and displacement magnitude would inevitably increase the registration error, since rotation and (subpixel) translation of the spindle involves interpolation which would propagate to subsequent frames. Our registration algorithm only uses the retardance images, which have a higher dynamical range and more pronounced internal features than the orientation images.

Spindle mask. We obtain a mask for the spindle for each frame of the stack. A gamma adjustment of the image followed by a filter averaging is used to enhance the contrast between the spindle and the background. An overestimation of the spindle shape that includes bright features of the background is initially obtained by image thresholding. A sequence of morphological operations, erosion followed by dilation, eliminates the remaining small features of the background and softens the boundary of the spindle. For binary images, erosion sets a pixel value to zero unless it is surrounded by a defined amount of ones, while dilation in a pixel of value one, sets the value of a defined neighboring pixels to one. The result of these operations is illustrated in Fig. 3B. The mask is multiplied by the image to filter the background prior to the correlation. We use the center of mass of the spindle mask to set a default translation of each frame to be improved by the correlation method.

Correlation between frames. Computing correlations directly on the filtered images is problematic because this procedure tends to maximize overlap of the masked regions, irrespective of their internal features, resulting in the same poor alignment as the spindle shape based algorithm described above. Better performance can be achieved by using distinctive internal features of the spindles, long-lived fluctuations in intensity or the presence of structure and ordering in the microtubules (bundling), to register consecutive frames. Therefore, we align the normalized fluctuations of the masked images instead of the masked images themselves,

$$\delta i_l = M_l \cdot \frac{I_l - \langle I_l \rangle}{\langle I_l \rangle}, \tag{1}$$

where l refers to the frame number, and the average is taken over the interior of the spindle defined by the mask M_l. It is necessary to normalize the correlation of the fluctuations by the area of shape intersection, Fig. 3C, to avoid bias due to the particular shape of the spindle or the algorithim for selecting the masked region. Using Fast Fourier Transforms (FFT) to speed computation, we can define the correlation as a function of angle of rotation θ and translation (l_x, l_y),

$$C(\theta, l_x, l_y) = \frac{F^{-1}\left[F[\delta i_{l-1}] \cdot F^*[R(\delta i_l, \theta)]\right]}{F^{-1}\left[F[M_{l-1}] \cdot F^*[R(M_l, \theta)]\right]}, \tag{2}$$

where $R(\delta i_l, \theta)$ is the rotation of the image δi_l by θ degrees, using cubic interpolation, and $(l_x, l_y) \in \mathbb{N}$. In order to find the maximum of the correlation as a function of translation and rotation, we discretize the angle θ from -10 to 10 in increments of 0.5 degrees. For each θ, we find (l_x, l_y) that maximizes the correlation in Eq. 2, and obtain a new correlation $C(\theta)$ that is a function of the rotation angle only. We find the angle θ_m that maximizes the correlation by finding the local maxima of the spline-interpolant of $C(\theta)$, Fig. 3D. Finally, using the value of the spindle orientation θ_m, we recalculate the correlation given by Eq. 2, and find the final translation (l_x, l_y) that align the two frames. Once this procedure is finished for the entire stack of images, all frames are registered at once. Since microtubules in the spindle are oriented on average along the spindle long axis, we add an offset to the rotation angle for each frame rotation that sets the mean microtubule orientation with respect to the horizontal of the image to 0. The result of the alignment procedure is illustrated in Fig. 2.

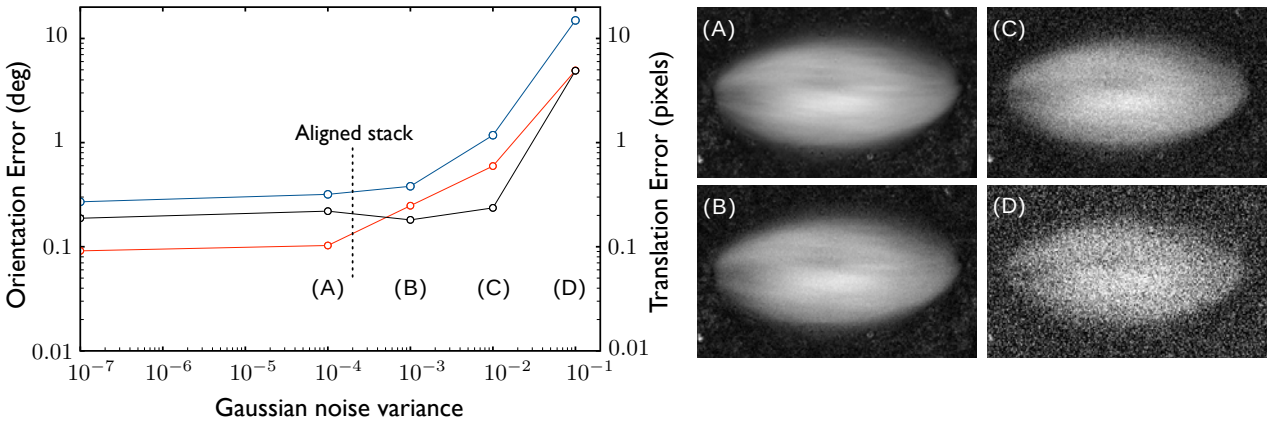

Figure 4. Characterization of the robustness of the alignment algorithm. The absolute error (standard deviation) in orientation (solid black, left axis), translation along the spindle long axis (blue, right axis), and translation along the spindle short axis (right axis), is obtained by rotating, translating, and adding white gaussian noise with different variance to an image. The range of rotation is $(-8, 8)$, and the range of translations is (-10,10). Each point is obtained from 100 random rotations and translations, and displayed in a log log scale. In order to easily understand the magnitude of the variance with respect to the intensity, the original image is rescaled to [01]. The alignment procedure is very robust for variances up to 10^{-1}, where the error increases by an other of magnitude. For reference, the noise added spindle images for different variances are displayed in the right panel (A), (B), (C) and (D). An aligned spindle series has an equivalent variance of 2×10^{-4}, which is well into the robust region, corresponding to an orientation error of ~ 0.2 deg (~ 0.004 rad), and translation error of $\sim 0.1 - 0.3$ pixels. Note that the error is larger along the spindle long axis, since the internal structures along this direction are less pronounced and defined.

Error estimation. The resulting stack of images from the registration algorithm appears to be very well aligned, Fig. 2, but it is desirable to have a more objective means to evaluate its performance. Unfortunately, as discussed above, there is not an unambiguous criterion to determine the quality of alignment since each image is different from the rest. One way to estimate the reliability of our algorithm is to try to register an image with itself after a certain level of noise and an arbitrary rotation and translation are applied. In the absence of information regarding the true statistics of variation between two consecutive images of the spindle, we use Gaussian white noise as the source of variability.

We calculated the absolute error in registration while varying the variance of the Gaussian noise by seven orders of magnitude and applying random rotations and translations (n=100 for each variance magnitude), Fig. 4. Fig. 4 shows representative images of a spindle with different levels of added noise. The registration algorithm is very robust for the three first spindles (A), (B) and (C). The absolute error is surprisingly small for at least five orders of magnitude in the value of the variance, and corresponds to an orientation error of ~ 0.2 deg (~ 0.004 rad), and translation errors of less than half a pixel. Notice that the level of noise in spindle (C) is already very large, and definitely an overestimate of the noise present in the real data. When the variance of the added noise is raised further and surpasses a threshold level, 0.1 if the retardance of the image is normalized to lie between 0 and 1 (corresponding to (D)), the error increases an order of magnitude and the algorithm fails.

We estimate the equivalent noise level of our images by calculating the variance between consecutive frames for an entire movie. We find that the variance of the oriented images is 2×10^{-4} (with retardance normalized to lie between 0 and 1). Added Gaussian noise with this variance is well within the robust region, and would result in an orientation error of ~ 0.2 deg (~ 0.004 rad), and translation error of $\sim 0.1 - 0.3$ pixels. This error estimation method suggests that our registration algorithm is quite accurate and can be safely used when calculating correlation functions. However, it is important to emphasize that this only provides an estimate the alignment error, since the real variation between consecutive images is not caused solely by Gaussian noise.

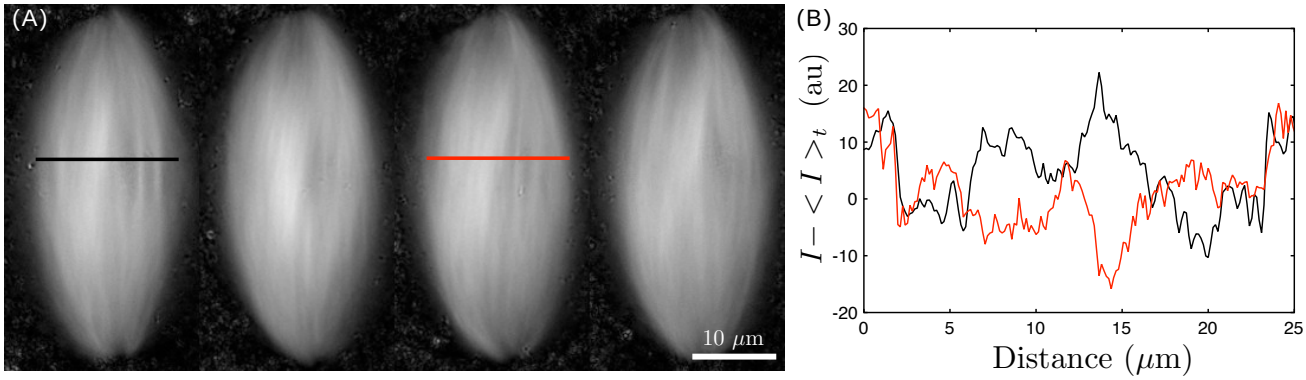

Figure 5. Retardance fluctuations in the spindle. Series of four retardance images at different times (0, 64, 130 and 198 seconds) (A), showing high spatial inhomogeneities which change on time. In (B) profile plot of the spatial fluctuations of images 1 (solid black) and 3 (solid red) corresponding to times 0 and 130 seconds respectively. Fluctuations over time change dramatically and actually seem to be inverted over time.

4. CALCULATION OF CORRELATION FUNCTIONS

Once the spindle images are properly registered, we can start comparing retardance and orientation of different points in the spindle at different times. There are massive fluctuations across space and time in both orientation and retardance, Fig. 5. Calculating correlation functions of fluctuations provides a powerful way of characterizing their behavior.[17,18] In the following we discuss methods to estimate the correlation function of an arbitrary process, and later on we will focus on the expression for the correlation of the fluctuations in microtubule orientation.

Estimation of the correlation function. We define the non-normalized spatiotemporal correlation function of a process $A(x, y, t)$ as[18]

$$c(\eta, \xi, \tau) = \langle \delta A(x, y, t) \delta A(x + \eta, y + \xi, t + \tau) \rangle, \tag{3}$$

where $\delta A(x, y, t)$ is a fluctuation around the mean $\langle A \rangle^*$ at position (x, y) and time t. Since the sampling in any experiment is finite, we can only obtain an estimate of the true correlation function. It is important to find a good estimate that is as close as the real correlation as possible. We first discuss methods of estimating the correlation function for a unidimensional process, following Percival and Walden.[19] Once the method is defined, generalization to any dimension is straightforward.

There are two immediate ways to estimate the correlation function. The most natural estimator, often called the "unbiased" estimator is defined as

$$c_u(\eta) = \frac{1}{N - |\eta|} \sum_{j=1}^{N-|\eta|} (A(j) - \langle A \rangle)(A(j + |\eta|) - \langle A \rangle), \tag{4}$$

If the mean of the process $\langle A \rangle$ obtained from N sample values, is substituted by the true mean μ, the above estimator is by definition an unbiased estimator. However, in most situations the true mean is unknown and an estimate of μ is must be obtained by averaging over the finite realizations of A. In this case, c_u is biased.

There is an alternative estimator of the correlation function called the "biased" estimator,

$$c_b(\eta) = \frac{1}{N} \sum_{j=1}^{N-|\eta|} (A(j) - \langle A \rangle)(A(j + |\eta|) - \langle A \rangle). \tag{5}$$

*Depending on the process it might be convenient to normalize the correlation function.

The only difference between the above estimators is the multiplicative factor in front of the summation. The magnitude of the bias on the later increases as $|\eta|$ increases. In the literature the "biased" estimator is preferred to the "unbiased" estimator. Here we will briefly motivate the reasons to use an estimator that is, by definition, biased. In the majority of occasions, the mean of the process must be accessed by averaging a finite number of samples, in which case both estimators are biased and in fact, the magnitude of the bias in c_u can be greater than in c_b.[19] In order to illustrate the later statement, consider the case of a white noise process with unknown mean μ and variance σ^2 . It can be easily shown that for this case the magnitude of the bias for c_u is $-\frac{\sigma^2}{N}$, while for c_b, the magnitude of the bias is $-\left(1-\frac{|\eta|}{N}\right)\frac{\sigma^2}{N}$, the later being smaller for any lag η. More generally, the variability in the "unbiased" estimator is worse than the inherent bias in the "biased" estimator. This effect is particularly important for $|\eta|$ approaching N where the variance of $c_u(N-1)$ is N^2 times the variance of $c_b(N-1)$.

For most physical processes of interest, $c(\eta)\to 0$ as $\eta\to\infty$. Although it is not a strong argument in favor of the "biased" estimator, this behavior is incorporated in it by definition. As an example, consider the nice decaying behavior of the temporal decay of the peak of the correlation function of the alignment in the spindle for the "biased" estimator in Fig. 6 as compared to the "unbiased" estimator whose amplitude for large time lag is unphysically greater than the amplitude for time lag 0. Finally, only c_b can calculated in terms of Fourier transforms (see below), which dramatically speeds the computational time. For the rest of the paper, we will use the generalization to higher dimensions of the "biased" estimator in Eq. 5 to estimate our spatio-temporal correlation function.

Correlation functions of physical processes are conveniently expressed in Fourier space. It can be shown that for the "biased" estimator (only),[19]

$$\begin{aligned} C(\vec{q},t) &= \sum_{\eta=-(N_x-1)}^{N_x+1}\sum_{\xi=-(N_y-1)}^{N_y+1} c(\eta,\xi,t)\exp(-i2\pi q_x\eta)\exp(-i2\pi q_y\xi) \\ &= \frac{1}{N_t}\sum_{t=1}^{N_t-\tau}\mathrm{Re}\left(F\left[\delta A(x,y,t)\right]F^*\left[\delta A(x,y,t+\tau)\right]\right). \end{aligned} \tag{6}$$

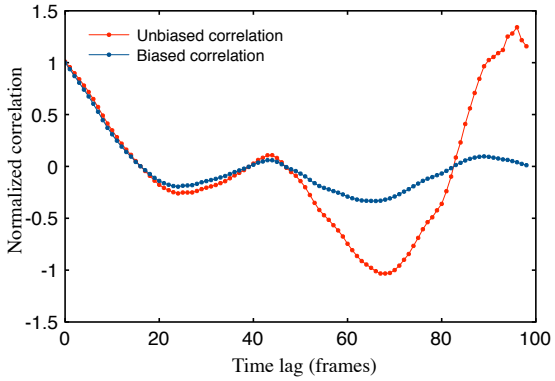

Figure 6. Comparison of the "biased" and "unbiased" estimators for the temporal decay of the peak of the correlation function of the alignment in the spindle. The "biased" estimator (blue curve) decays nicely to 0 as the lag increases, while the "unbiased" estimator shows unphysical behavior for large time lags.

Microtubule orientation order parameter. The images obtained with the LC-Polscope, Fig. 1, contain information on the retardance and orientation of microtubules in the spindle. This technique cannot determine the polarity of microtubules. As a consequence, microtubules under the LC-Polscope have the same order

parameter properties as a nematic, this is, the directions $\hat{n}$ and $-\hat{n}$ are equivalent. The proper way to define the order parameter is not by using the orientation angle, but a traceless tensorial order parameter,[20]

$$Q_{\alpha\beta} = \left(n_\alpha n_\beta - \frac{1}{2}\delta_{\alpha\beta} \right) = \frac{1}{2} \begin{pmatrix} \cos 2\theta & \sin 2\theta \\ \sin 2\theta & -\cos 2\theta \end{pmatrix}, \tag{7}$$

where $\hat{n} = (\cos\theta, \sin\theta)$, and we have assumed a two dimensional order parameter. Using the expression for the correlation function, Eq. 6,

$$C_Q(\vec{q}, t) = \frac{1}{N_t} \sum_{t=1}^{N_t - \tau} \mathrm{Re}\left(F\left[\delta Q_{\alpha\beta}(\vec{x}, t)\right] F^*\left[\delta Q_{\alpha\beta}(\vec{x}, t+\tau)\right] \right) \tag{8}$$

$$= \frac{1}{2N_t} \sum_{t=1}^{N_t - \tau} \mathrm{Re}\left(F[\delta \cos 2\theta(\vec{x}, t)] F^*[\delta \cos 2\theta(\vec{x}, t+\tau)] + F[\delta \sin 2\theta(\vec{x}, t)] F^*[\delta \sin 2\theta(\vec{x}, t+\tau)] \right), \tag{9}$$

where summation over repeated indices is assumed. Normalization of the correlation function is not needed since the nematic order parameter is unitary by definition. Finally, we need to decide how to estimate the mean of the order parameter, and correspondingly the fluctuations. In order to avoid spatial inhomogeneities in the orientation inherent of the spindle shape, we calculate the fluctuations at any point in the spindle by substracting the temporal mean of the order parameter at that point, $\langle Q_{\alpha\beta}(\vec{x}) \rangle \equiv 1/N_t \sum_{t=1}^{N_t} Q_{\alpha\beta}(\vec{x}, t)$. One cut of the correlation function is displayed in Fig. 6.

5. CONCLUSIONS

We have proposed a method to measure fluctuation correlations in the microtubule orientation of metaphase spindles. We have presented a registration algorithm, explored its robustness and conclude that it satisfactorily corrects for spindle motions during acquisition. Finally, we have discussed and derived the expression that estimates the correlation function of the nematic order parameter of microtubules that form the spindle. Further studies of the form of the correlation function will provide insights into the dynamics of the spindle and quantitative tests of the validity of coarse-grained models.

ACKNOWLEDGMENTS

JB acknowledges the support of the Human Frontier Science Program. DJN acknowledges the support of a grant from the Nation Science Foundation (PHY0847188).

REFERENCES

[1] Mitchison, T. J. and Salmon, E. D., "Mitosis: a history of division," *Nature Cell Biology* **3**, E17–E21 (2001).

[2] Mitchison, T. J., "Mechanism and function of poleward flux in xenopus extract meiotic spindles," *Philosophical Transactions of the Royal Society B* **360**, 623–629 (2005).

[3] Gadde, S. and Heald, R., "Mechanisms and molecules of the mitotic spindle," *Current Biology* **14**, R797R805 (2004).

[4] Chaikin, P. and Lubensky, T. C., [*Principles of condensed matter physics*], Cambridge University Press (1995).

[5] Kruse, K., Joanny, J. F., Julicher, F., Prost, J., and Sekimoto, K., "Asters,vortices, and rotating spirals in active gels of polar filaments," *Physical Review Letters* **92**(7), 078101 (2004).

[6] Lee, H. Y. and Kardar, M., "Macroscopic equations for pattern formation in mixtures of microtubules and molecular motors," *Physical Review E* **64**, 056113 (2001).

[7] Liverpool, T. B. and Marchetti, M. C., "Instabilities of isotropic solutions of active polar filaments," *Physical Review Letters* **90**(13), 138102 (2004).

[8] Aranson, I. S. and Tsimring, L. S., "Pattern formation of microtubules and motors: inelastic interaction of polar rods," *Physical Review E* **71**, 050901 (2001).

[9] Sato, H., Ellis, G. W., and Inoue, S., "Microtubular origin of mitotic spindle from birefringence," *The Journal of Cell Biology* **67**, 501–517 (1975).

[10] Inoue, S., "Organization and function of the mitotic spindles," *Primitive Motile Systems in Cell Biology* **549** (1964).

[11] Gov, N. S. and Safran, S. A., "Red blood cell membrane fluctuations and shape controlled by atp-induced cytoskeletal defects," *Biophysical Journal* **88**, 18591874 (2004).

[12] Oldenbourg, R., "A new view on polarization microscopy," *Nature* **381**, 811–812 (1996).

[13] Murray, A. W., "Cell cycle extracts," in [*Methods in Cell Biology*], Kay, B. K. and Peng, B., eds., 581–605, Academic Press (1993).

[14] Hannak, E. and Heald, R., "Investigating mitotic spindle assembly and function in vitro using xenopus laevis egg extracts," *Nature Protocols* **1**(5), 2305–2314 (2006).

[15] Reddy, B. S. and Chatterji, B. N., "An fft-based technique for translation, rotation, and scale-invariant image registration," *IEEE Transactions on Image Processing* **5**(8), 12661271 (1996).

[16] Brown, L. G., "A survey of image registration techniques," *ACM Computing Surveys* **24**(4), 325–376 (1992).

[17] Elson, E. and Magde, D., "Fluorescence correlation spectroscopy. i. conceptual basis and theory," *Biopolymers* **13**, 1–27 (1974).

[18] Kolin, D. L. and Wiseman, P. W., "Advances in image correlation spectroscopy: Measuring number densities, aggregation states, and dynamics of fluorescently labeled macromolecules in cells," *Cell Biochem Biophys* **49**, 141–164 (2007).

[19] Percival, D. and Walden, A. T., [*Spectral Analysis for Physical Applications*], Cambridge University Press (1993).

[20] de Gennes, P. G. and Prost, J., [*The Physics of Liquid Crystals*], Oxford Science Publications (1993).